RSC Advances

ROYAL SOCIETY OF CHEMISTRY

www.rsc.org/advances

Graphical abstract

Coulomb block effect inducing distinctive dielectric properties in electroless plated barium titanate@silver/poly(vinylidene fluoride) nanocomposites

Li Ren[a], Xing Meng[a], Jun-Wei Zha[a†], Zhi-Min Dang[a,b†]

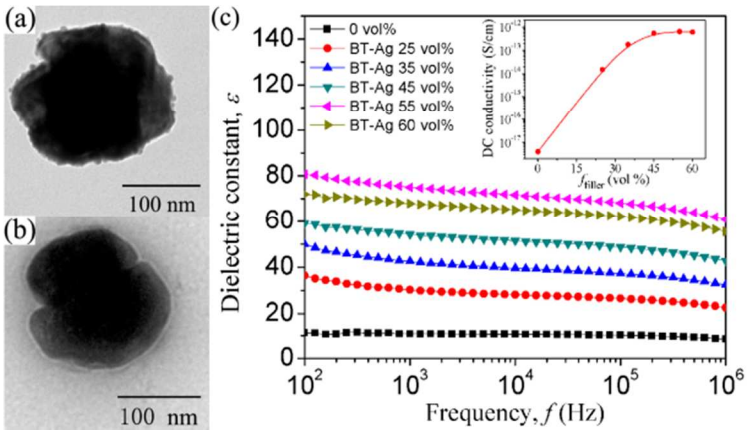

The BT@Ag particles (a) were prepared by electroless plating to deposit Ag nanoparticles on the surface of BT (b). The BT@Ag/PVDF composites have high dielectric constant and the direct current conductivity keeps in the order of 10^{-12} S/cm when the filler content is more than 35 vol% (c).

Journal Name

ARTICLE

Coulomb block effect inducing distinctive dielectric properties in electroless plated barium titanate@silver/poly(vinylidene fluoride) nanocomposites

Received 00th January 20xx,
Accepted 00th January 20xx

DOI: 10.1039/x0xx00000x

www.rsc.org/

Li Ren[a], Xing Meng[a], Jun-Wei Zha[a†], Zhi-Min Dang[a,b†]

Silver (Ag) nanoparticles with an average diameter of 5~10 nm were dotted on the surface of barium titanate ($BaTiO_3$, BT) by electroless plating. The poly(vinylidene fluoride) (PVDF) nanocomposites filled with BT@Ag hybrid particles were prepared by solution method. Transmission electron microscopy and X-ray diffraction observations revealed that the Ag nanoparticles were well dotted on the surface of BT nanoparticles, and there was no phase transformation of BT could be observed. Differential scanning calorimetry results showed that the degree of crystallinity and melting temperature decrease with the increasing content of filler. Breakdown strength of the BT@Ag/PVDF composites as well as BT/PVDF decreased with the increasing volume fraction (f_{filler}) of fillers. Dielectric constant of BT@Ag/PVDF composites was gradually increased with the increasing f_{filler} of BT@Ag from 0 to 55 vol%, while a little decrease when f_{filler} up to 60 vol%. It was worth noting that the dielectric constant of BT@Ag/PVDF composites was higher than that of BT/PVDF composites with the same f_{filler}, and the dielectric loss of BT@Ag/PVDF composites kept low. The direct current conductivity of the BT@Ag/PVDF composites had a significant dependence on the concentration of BT@Ag and kept in the order of 10^{-12} S/cm when f_{filler} was more than 35 vol%. These may be ascribed to the small size of Ag nanoparticles and the Coulomb block effect.

1. Introduction

Dielectrics are vital in nearly all electronic devices and microelectronics areas. The common uses include the dielectric capacitors, dielectric filtering, packaging technology and so on.[1-3] Ceramic materials used as the traditional dielectric materials possess high dielectric constant. However, its high density, brittleness and challenging processing conditions greatly restrict its practically application in modern industry.[1] Dielectric polymer materials have gained great attention in the past decades due to the excellent physical and chemical properties, such as low density, mechanical flexibility, easy processing, which balanced the disadvantages of ceramic materials.[4-5] However, generally the dielectric constant of common polymers is low, striving to significantly improve the dielectric constant of polymers have been an issue in the dielectric polymer materials. Therefore, polymer composites with unique dielectric properties have attracted tremendous attention due to these composites retain the high dielectric constant of ceramic materials and the advantages of polymer matrix. The common method is known to adopt ceramic particles or conductive materials as fillers, such as barium titanate ($BaTiO_3$, BT).[6-8] calcium copper titannate ($CaCu_3Ti_4O_{12}$, CCTO),[9] carbon nanotube (CNT),[10-12] zinc-zinc oxide (Zn-ZnO) particles.[13] However, the high filler loadings for these composites are usually needed in order to realize higher dielectric constant for the practical application, which induced poor mechanical performance, low flexibility and the agglomeration of nanoparticles.[14] For the conductive fillers, it is used as an additive to raise the dielectric constant of the polymer matrix by the percolation theory.[15-16] Namely, when the content of conductive filler is near the percolation threshold (f_c), the dielectric constant of the polymer composite always demonstrates an abrupt increase. Generally, the addition of conductive fillers enhances the dielectric constant of polymer composites while causes the high dielectric loss and high electrical conductivity simultaneously. Therefore, it is necessary to exploit a method for the fabrication of polymer-based composites with unique dielectric properties and low electrical conductivity.

In this work, BT@Ag hybrid particles were prepared by the electroless plating, and the Ag nanoparticles were dotted on the surface of $BaTiO_3$ nanoparticles. The popular dielectric polymer,

[a] Laboratory of Dielectric Polymer Materials and Devices, Department of Polymer Science and Engineering, School of Chemistry and Biological Engineering, University of Science and Technology Beijing, Beijing 100083, P. R. China
[b] State Key Laboratory of Power System, Department of Electrical Engineering, Tsinghua University, Beijing 100084, China
†Author to whom correspondence should be addressed; electronic mail: zhajw@ustb.edu.cn; dangzm@tsinghua.edu.cn.

Electronic Supplementary Information (ESI) available: [details of any supplementary information available should be included here]. See DOI: 10.1039/x0xx00000x

poly(vinylidene fluoride) (PVDF), was used as the matrix attribute to its ferroelectric superiority with relative higher dielectric constant among the polymer families. The BT@Ag/PVDF composite was prepared by the method of solvent blend, containing the hybrid nanoparticles dispersed in the PVDF matrix with different volume fraction (f_{filler}) from 25 vol% to 60 vol%, and their dielectric properties were investigated. For comparison, the crude BT particles filled in the PVDF matrix were also prepared with filler content of 25 vol%, 45 vol% and 60 vol%, respectively. The introduction of metal nanoparticles on the surface of BT gives the composite excellent dielectric properties and low conductivity. Compared with BT/PVDF composite, the BT@Ag/PVDF composites possess higher dielectric constant with the same filler content. Temperature dependence of dielectric properties and alternating current (AC) conductivity on the two kinds of PVDF composites was also studied that some differences in high temperature range were found. These results can be explained in terms of the special properties of nano-Ag ranged from 5~10 nm and the Coulomb block effect.

2. Experimental

2.1 Preparation of the BT@Ag particles

The BT (ca. 100 nm) nanoparticles were provided by Aladdin. The BT@Ag hybrid particles were prepared by electroless plating to deposit Ag nanoparticles on the surface of BT. Prior to the electroless plating, the BT nanoparticles were firstly sensitized with $SnCl_2$ acidic solution.[17] And then the depositing process was taken in the Rochell salt plating bath, which is a mixture of bath A and bath B in accordance with practice.[18] In consideration of the better dispersion of BT in ethanol and the electroless plating of silver in protonic solvent, both of the two bathes solvent were chosen as H_2O/ethanol (v/v=8:2), instead of H_2O only. Taking the theoretical calculated mass ratio of BT/Ag = 90/10 for example, 3 g BT was dispersed in bath A with 10 ml of 0.2 M silver ammonia solution, following by low-speed agitation and ultrasonic treatment for 30 min. Afterward equal volume of bath B was added to the brown dispersion with high-speed agitation constantly, bath B involved 0.7 M of potassium sodium tartrate and 0.9 M of $MgSO_4$ in the mixed solvent. After reacting 2 h at room temperature, the dark brown dispersion was centrifuged at 4000 rpm for 15 min. The precipitate was washed three times with H_2O/ethanol by centrifugation. After drying the precipitate under vacuum at 60 ^oC for 4 h, strong brown powder, namely, BT@Ag was obtained. In the similar way we can prepare series mass ratios of composite particles by tuning the concentration of plating bath. In this work, we had concluded that the mass ratio of silver in the BT@Ag is 5.0 wt% which was determined by Volhard method (ISO 1841).

2.2 Modification of the BT@Ag and BT nanoparticles

To make sure the excellent compatibility between the fillers and the polymer matrix, the surface of BT@Ag and BT nanoparticles were modified by γ-aminopropyltriethoxy silane (KH550), respectively.[19-20] Firstly, BT@Ag nanoparticles were mixed with 5.0 wt% KH550 in toluene media by refluxing for 5 h. Secondly, the mixtures were washed with deionized water and ethanol for several times. And then the cleaned precipitate was dried in vacuum oven. Finally, the modified BT@Ag nanoparticles with KH550 were obtained. The BT nanoparticles were modified by the same procedures.

2.3 Preparation of the PVDF nanocomposites

Compositing the filler powders with the PVDF (Shanghai 3F Company, China) was carried by the following steps. PVDF powders were dried completely in a vacuum oven at 80 °C overnight before using. Then the modified BT@Ag particles with various volume ratios were ultrasonic dispersed in N, N-dimethylformamide (DMF, Beijing Chemical Works, China) for 30 min. PVDF powders with predetermined weights was added and the mixture was acutely stirred in water bath of 70 ^oC for 5 h to ensure the complete dissolution of PVDF, and then the mixture was casted on a clean glass plate and subsequently heated at 70 ^oC for 7 h under vacuum. Finally, a film around 30 μm in thickness was obtained. The BT/PVDF composites prepared with a similar procedure.

2.4 Characterization

X-ray diffraction measurements were performed on a DMAXRB 12 kW diffractometer (Rigaku, Japan) with the K ray of Cu (the wavelength is 0.15406 nm). The scanning voltage and current were 40 kV and 150 mA, respectively. The measured 2θ range was 10-100° with a scanning interval of 0.02° and scanning rate of 10.0 ° min^{-1}. The Fourier transform infrared (FT-IR) spectra were measured by using a Nicolet 6700 spectrometer over the range of 4000 to 500 cm^{-1}.

The morphologies of pristine BT nanoparticles, sensitized BT nanoparticles and electroless plated BT nanoparticles with 5 wt% of silver were characterized by transmission electron microscopy (TEM, Hitachi H-7650B, Japan), respectively. A mixture of a small amount of nanoparticles in alcohol was sonicated at room temperature for 30 min. Then the obtained dispersion was dropped on a copper grid, and dried at room temperature before the TEM observation. The PVDF-based composites were fractured in liquid nitrogen and then the fractured surface was sputtered with gold for scanning electron microscopy **(**SEM, S4700, Hitachi, Japan) observation with an accelerating voltage of 20 kV.

Differential scanning calorimetry (DSC) measurements were performed using a DSC-60 (Shimadzu, Japan) in nitrogen atmosphere. Temperature and enthalpy were calibrated with indium. The samples of 4-6 mg were sealed in aluminum crucibles. The samples were first heated to 200 ^oC at 10 ^oC min^{-1} and kept isothermal for 3 min to eliminate the complex thermal history. Then they were cooled to 30 ^oC at 10 ^oC min^{-1} and kept isothermal for 3 min. Subsequently, they were heated again to 200 ^oC at 10 ^oC min^{-1}. Dielectric properties and alternating current (AC) conductivity of the samples were performed by Agilent 4294A impedance analyzer in the frequency ranges from 10^2 to 10^6 Hz at room temperature and the temperature ranges of -40 ~120 ^oC, respectively. Both sides of the samples in square shape with area of ca. 1.0 cm^2 were coated with silver as electrodes before testing. Direct current (DC) electrical conductivity of the samples were tested by high resistance meter (HRM, Keithley 6517B).

Journal Name

ARTICLE

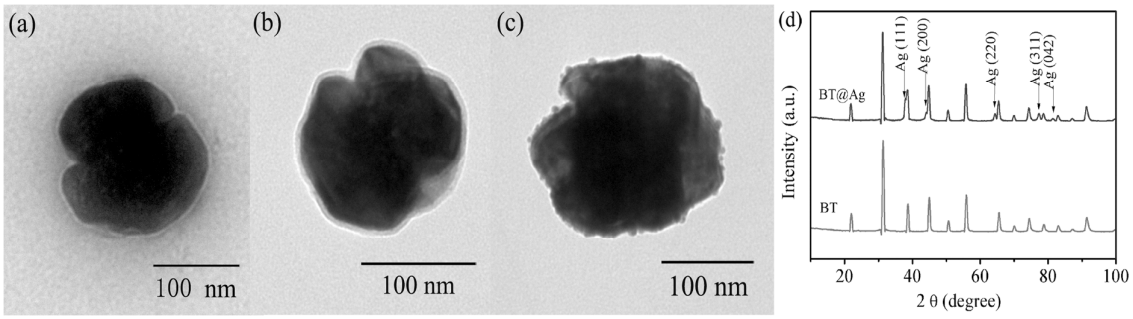

Fig. 1 TEM images of (a) $BaTiO_3$, (b) sensitized $BaTiO_3$, and (c) electroless plated $BaTiO_3$ nanoparticles with 5 wt% of silver, respectively. (d) XRD pattern of BT@Ag and BT particles.

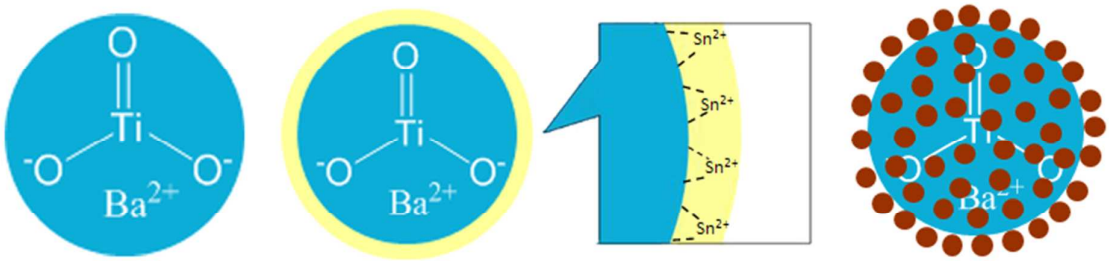

Fig. 2 Schematic illustration of the process of sensitization and electroless plating of $BaTiO_3$ (not to scale).

The breakdown strength of the composites was tested in a heat-transfer fluid bath at room temperature with a CS2674A high-voltage amplifier under a ramp rate of 200 V s^{-1}. The samples were located between two electrodes and immersed in silicone oil. The samples thickness was measured three times near the failure point, and the average was considered for calculation. At least 10 data points for each sample were collected and the average value was calculated.

3. Results and discussion

Figs. 1a-1c present TEM images of (a) BT, (b) sensitized BT, and (c) electroless plated BT nanoparticles with 5 wt% of silver, respectively. Comparing the morphologies of BT before and after sensitizing treatment (Fig. 1a and Fig. 1b), it can be clearly seen that there is a shell on the sensitized BT. In Fig. 1c, it can be seen that some particles are dotted on the shell, indicating some silver particles are successfully attach on the surface. XRD spectrum of BT@Ag and BT particles are shown in Fig. 1d. After electroless plating, the powder (upper curve) is identified as silver by the five small new diffraction peaks according to the literature.[21] The rest diffraction peaks come from BT, as the XRD spectrum of BT before plating (lower curve) shows the same diffraction peaks. This demonstrates the formation of Ag and no phase transformation of BT through the process of sensitization and electroless plating. Therefore, it can be illustrated by the following schematic as shown in Fig. 2. The Sn^{2+} irons are absorbed on the surface of BT by electrostatic interaction with the negative charges on the BT. Then the Sn^{2+} irons act as the starting point for growth of silver by reducing $[Ag(NH_3)_2]^+$ to initial Ag dot. With the help of a chemical reducing agent, more silver would deposit on the surface of BT nanoparticles by autocatalysis.

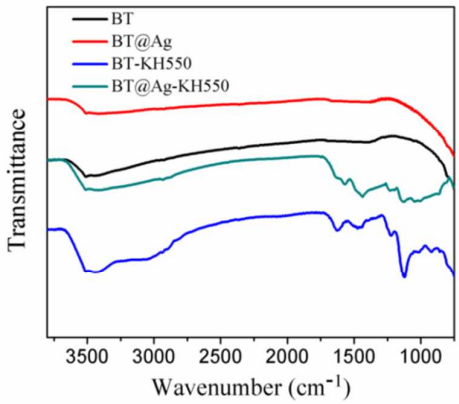

Fig. 3 FT-IR spectra of BT, BT@Ag, BT with KH550 and BT@Ag with KH550.

The FT-IR spectra of BT, BT@Ag, BT with KH550, and BT@Ag with KH550 are shown in Fig. 3. The peaks at ca. 3520 cm^{-1} for BT and BT@Ag may be associated with the stretching of O-H. However, compared to pristine BT, a weak absorption band at 3520 cm^{-1} in the spectrum of BT@Ag can be clearly observed, which may be because the process of sensitization and electroless plating influences the existence of hydroxyl groups on BT surfaces. The peaks at ca. 3503 cm^{-1} and 3422 cm^{-1} for BT with KH550 and BT@Ag with KH550 may be assigned to the stretching of N-H, and the peak at 1128 cm^{-1} may be assigned to the stretching of C-N. Meanwhile, the peak of the vibration of N-H occurs at 1624 cm^{-1} and 1567 cm^{-1} for BT with KH550 and BT@Ag with KH550, respectively. Those results indicate that successful animation of the fillers by reacting with KH550.

Figs. 4a-4f present the morphologies of fractured surfaces of BT/PVDF and BT@Ag/PVDF composites with f_{filler} of 25 vol%, 45 vol% and 60 vol%, respectively. It can be seen that some pores and agglomeration of fillers in the composites when the f_{fille} is 60 vol%. This is because that PVDF can not completely fill up the space between the fillers when the percentage of PVDF becomes less. As a result, the agglomeration of fillers and pores in the composites are inevitable. High-magnification images of BT and BT@Ag embedded in the PVDF with the f_{filler} of 45 vol% are shown in the inset in (b) and (e), which indicate that Ag particles still tightly stick to the surface of BT core through the strong mixing and film-casting process.

Fig. 5 shows the DSC curves of the BT/PVDF and BT@Ag/PVDF composites with different f_{filler} loading. The degree of crystallinity (X_c) for PVDF component is calculated by the equation as follow:

$$X_C = \frac{\Delta H_m}{w^{PVDF} \times \Delta H_m^{\infty}} \times 100\% \quad (1)$$

where ΔH_m is melting enthalpy measured by DSC during the second heating, ΔH_m^{∞} is the melting enthalpy of perfect PVDF crystals (104.7 J g^{-1}),[22] and w^{PVDF} is the weight fraction of PVDF. The corresponding data were summarized in Table 1. It can be seen that the melting temperature (T_m) and X_c of the BT/PVDF and BT@Ag/PVDF composites decrease with the increasing f_{filler} and the T_m and X_c of BT@Ag/PVDF composites are somewhat lower when compared with that of the BT/PVDF composites with the same f_{filler}. This may be because the addition of fillers prohibits the mobility of the polymer segments that result in the decrease of the degree of X_c and T_m and the effect is more pronounced for the BT@Ag/PVDF composites due to the attachment of Ag nanoparticles on the surface of BT. With the increasing f_{filler}, there are more aggregations of filler and some pores/defects emerge inside the sample, resulting in the further decrease of the X_c and T_m.

Frequency dependence of dielectric constant (ε), dielectric loss (tan δ), AC conductivity of the BT/PVDF and BT@Ag/PVDF composites with different f_{filler} at room temperature are shown in Figs. 6(a)-(c). As can be seen in Fig. 6a, the ε of BT@Ag/PVDF composites increases with the increasing f_{filler}. Differently, when f_{filler} is of 60 vol%, ε of the composites is lower than that of 55 vol%, as well as the AC conductivity, as shown in Fig. 6c. For the BT/PVDF composites, the trend of variation for ε and AC conductivity is similar to that of BT@Ag/PVDF composites, namely the ε and AC conductivity increase with the increasing f_{filler} when the f_{filler} is 25 vol% and 45 vol%. While the ε and AC conductivity slight decrease when the f_{filler} is 60 vol%. The reason should be attributed to the aggregation of fillers and the pore and defect induced by the high inclusion concentration, as demonstrated in Figs. 5(c) and 5(f). It is worth noting that the ε of BT@Ag/PVDF composites is higher than that of BT/PVDF composites when the f_{filler} is same, especially in the high f_{filler}. This phenomenon can be understood in terms of the existence of Ag nanoparticles, which increases the electric charge transference.[23] The second most significant phenomenon is the

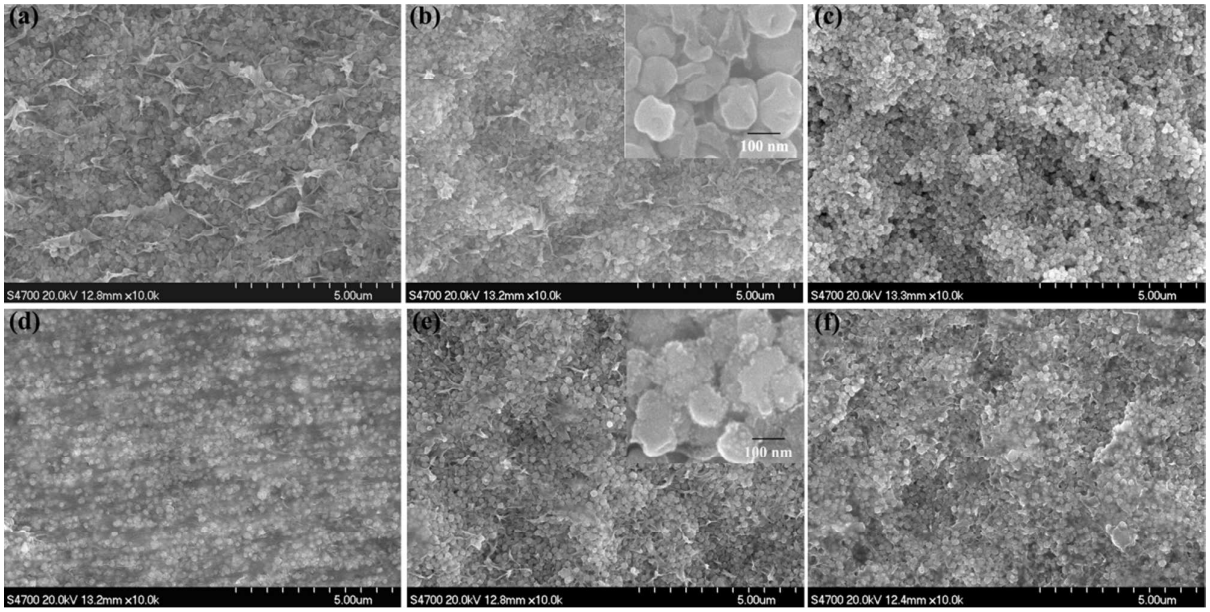

Fig. 4 Morphologies of fractured surfaces of BT/PVDF ((a), (b) and (c)) and BT@Ag/PVDF ((d), (e) and (f)) composites with different f_{filler}. The insets in (b) and (e) are the high-magnification images of BT and BT@Ag embedded in the PVDF with 45 vol% fillers loading.

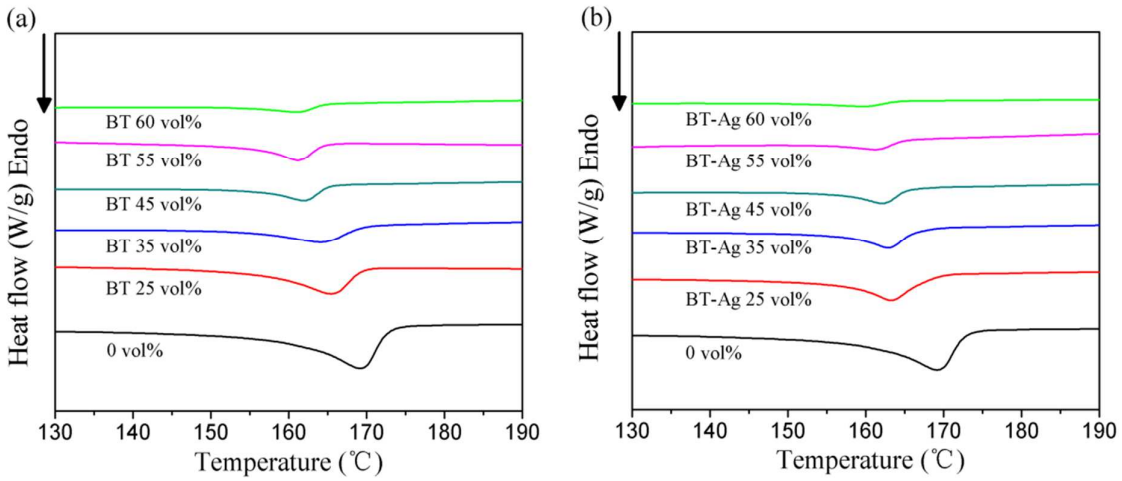

Fig. 5 DSC thermographs showing heat flow (HF) of (a) BT/PVDF and (b) BT@Ag/PVDF composites with differern f_{filler}.

Table. 1 The melting and crystallization data from DSC measurement for BT/PVDF and BT@Ag/PVDF composites with different f_{filler}. The data are obtained from Fig. 5 and calculated by equation (1).

Sample	Melting temperature T_m (°C)	Melting enthalpy ΔH_m (J g^{-1})	The degree of crytallinity, X_c (%)
PVDF	169.3	49.32	47.11
BT/PVDF 25 vol%	165.7	22.03	44.69
BT/PVDF 35 vol%	164.5	16.06	43.18
BT/PVDF 45 vol%	162.3	14.95	39.38
BT/PVDF 55 vol%	161.5	9.35	36.80
BT/PVDF 60 vol%	161.0	5.98	28.87
BT@Ag/PVDF 25 vol%	163.6	19.59	39.73
BT@Ag/PVDF 35 vol%	162.6	13.98	37.59
BT@Ag/PVDF 45 vol%	162.1	12.37	32.58
BT@Ag/PVDF 55 vol%	161.2	7.26	28.57
BT@Ag/PVDF 60 vol%	159.5	4.19	20.23

relative weak frequency dependence of ε for all the samples, even those with high loading of f_{filler}≥45 vol%. Besides, it worth noted that the tan δ of BT@Ag/PVDF composites remained at relative low level (Fig. 6b) below 1 MHz, which is in sharp contrast with that of the $BaTiO_3$-X/PVDF three-phase composites, in which X is the other filler with high electrical conductivity, such as carbon nanotube,[24] graphene,[25] conductive polyaniline.[26] According to percolation theory,[15-16] when the volume fraction of conductive filler is near the f_c, where the fillers connect with each other to form a continuous conducting path, making it possible that electrons or carriers transport among the fillers, consequently the composite always demonstrate an abrupt increase in electrical properties. However, the BT@Ag/PVDF composites in this work behave differently in spite of the existence of metal nanoparticles. Fig. 6(d) indicates the f_{filler} dependence of DC conductivity of the BT@Ag/PVDF composites. When the f_{filler} is up to 35 vol%, the DC conductivity is kept in the order of 10^{-12} S/cm, rather than increases rapidly. This phenomenon might be ascribed to the Coulomb block effect of Ag nanoparticles.[27-28] Metal particles with nanoscale in diameter show a unique property, namely, with an electron in insulation system they can establish a barrier of $e^2/2C$. If the barrier is far more than the energy of thermal motion of the electron, k_BT (k_B is the

Journal Name

ARTICLE

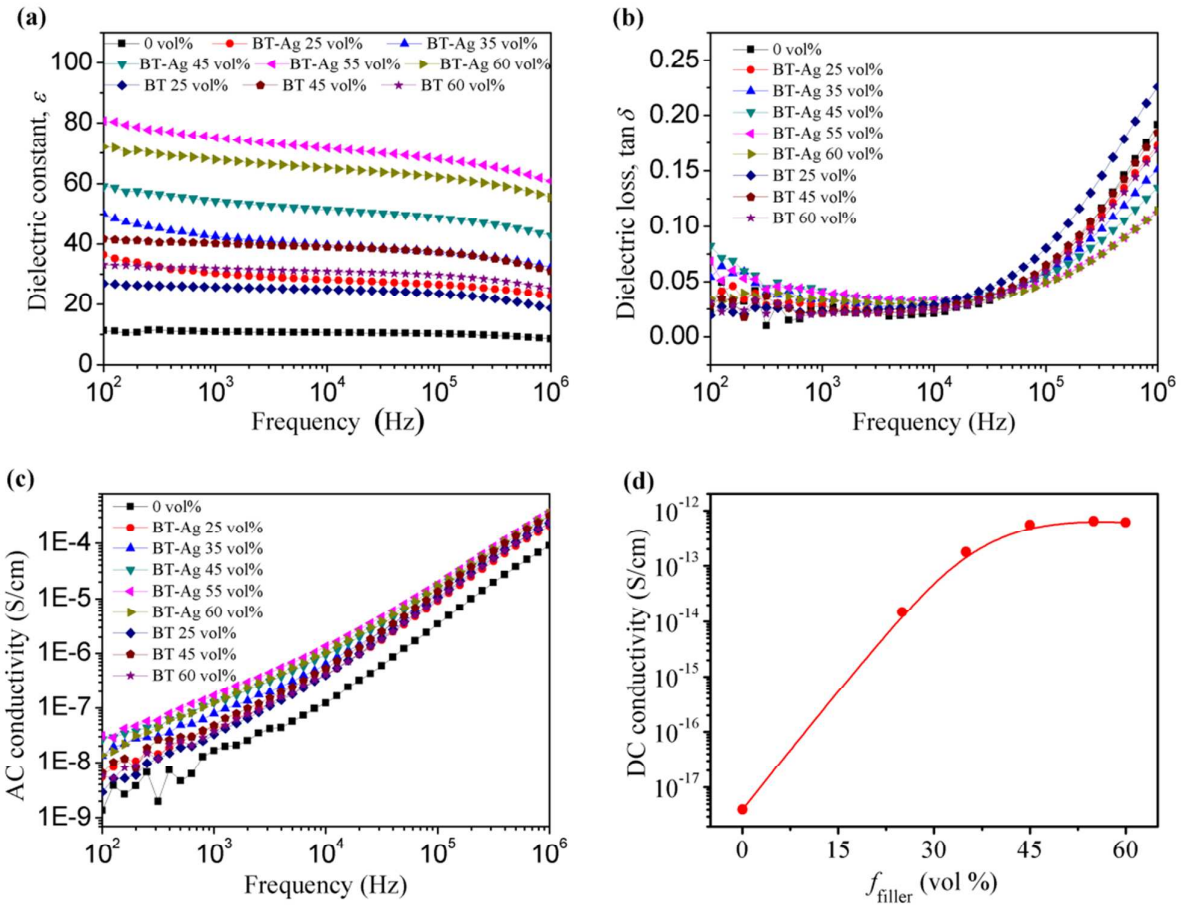

Fig. 6 Frequency dependence of the (a) dielectric constant, (b) dielectric loss, and (c) AC conductivity of the BT/PVDF and BT@Ag/PVDF composites with different f_{filler}, and (d) is the f_{filler} dependence of the DC conductivity of the BT@Ag/PVDF composites.

Boltzmann constant), it will prevent the second electron passing through, and the metal nanoparticle could be considered as Coulomb island.[29] In this study, when the Ag nanoparticles ranged from 5-10 nm, the electron in this system was hardly to depart from the Coulomb island due to the barrier, thus another electron was not easy to tunnel in materials. Thus, the composites was insulative, even when f_{filler} is as high as 60 vol% and Ag nanoparticles on adjacent BT are so close with each other.

Fig. 7 shows the temperature dependency of ε, tan δ and AC conductivity of pure PVDF, BT/PVDF and BT@Ag/PVDF composites with f_{filler}=55 vol% at 10^3 Hz. In Fig. 7a, as it can be seen, whether there is Ag or not, each of the two kinds composites shows larger ε than that of pure PVDF in whole temperature range. With the increasing temperature, the ε of pure PVDF and BT/PVDF composites increase softly and the ε of BT@Ag/PVDF increases obviously, especially in the temperature range of 70-120 °C. Besides, in Figs. 7b and 7c, we can see that tan δ and AC conductivity of the composites with Ag or not keep the same trend in temperature range of -40-70 °C. However, the trend becomes different, the tan δ and AC conductivity of the composites without Ag begin to flatten, while the composites with Ag keep the rising trend when the temperature rises from 70 to 120 °C. These results can be explained as follows: the expansion of the free volume in the polymer that makes the dipoles in the films orientating easily under the electric field which result in the increase of ε for the three samples with the increasing temperature. On the other hand, the k_BT is larger than the barrier of $e^2/2C$ in relative high temperature

Journal Name

ARTICLE

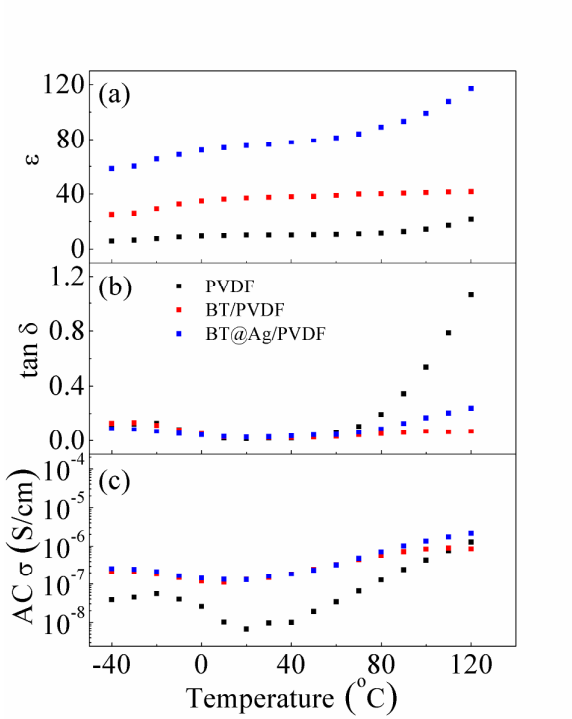

Fig. 7 Temperature dependence of (a) dielectric constant, (b) dielectric loss, and (c) AC conductivity of the composites with f_{filler}=55 vol% at 10^3 Hz.

range which results in the electron enters or leaves Coulomb island more easily. Thus，the Coulomb block effect is weakened so that more agitated electrons can tunnel and the tan δ and AC conductivity of the material increase.

Fig. 8 shows the breakdown strength of BT/PVDF and BT@Ag/PVDF composites with the different f_{filler} loading. It can be seen that the breakdown strength of composites decreases with the increasing f_{filler} and the breakdown strength of BT@Ag/PVDF composites is lower when compared with that of the BT/PVDF composites with the same f_{filler}, so do X_c and T_m. This because the breakdown strength highly depends on the defect density of the sample. With the increasing fillers loading, the degree of crystallinity of composites decreases and the phenomenon is more clearly in BT@Ag/PVDF composites, which can be seen in Table 1. The more amorphous region emerged inside the composites could result in more defects, thus the breakdown strength of the composites decreases clearly. On the other hand, when there are aggregations of filler and some pores emerge in the samples, the inhomogeneous electric filed intensity can be formed inside the composites under external electric field. Thus the composites are easy to be electrically broken down by the local discharge.[30]

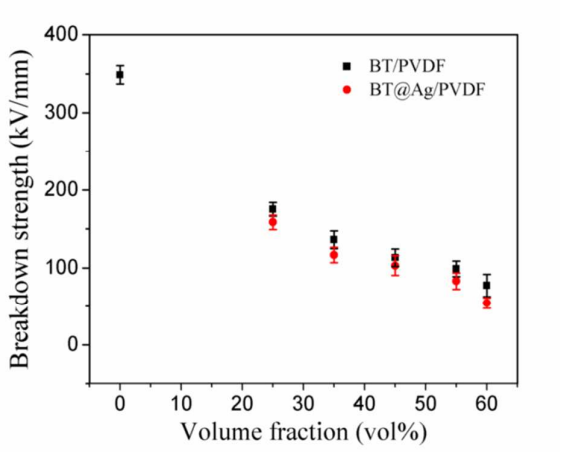

Fig. 8 Breakdown strength of the BT/PVDF and BT@Ag/PVDF composites.

4. Conclusion

In summary, Ag nanoparticles were dotted onto the BT nanoparticles by electroless plating. A composite was obtained by embedding these BT@Ag particles into PVDF matrix. Compared with the BT/PVDF composites, with the same filler content, the ε of BT@Ag/PVDF composites is higher and the tan δ has little change and kept low when the filler content is high. Besides, the degree of crystallinity, melting temperature and breakdown strength of the BT/PVDF and BT@Ag/PVDF composites decrease with the increasing f_{filler}. However, in BT@Ag/PVDF composites, because of the Coulomb block effect of Ag nanoparticles, when the filler content of BT@Ag particles is more than 35 vol%, with the increase of f_{filler}, the DC conductivity of BT@Ag/PVDF composites is kept in the order of 10^{-12} S/cm, rather than increases rapidly. For the temperature dependence of dielectric properties and AC conductivity, there are some differences between the BT@Ag/PVDF and BT/PVDF composites in high temperature range. This work could shed some light on better optimization of the polymer composites with unique dielectric properties.

Acknowledgements

This work was financially supported by NSF of China (Grant Nos. 51377010, 51425201 and 51207009), Ministry of Education of China through Doctor Project (Grant No. 20130006130002), the National Basic Research Program of China (973 Program) (Grant No. 2015CB654603), Fundamental Research Funds for the Central Universities (No. FRF-TP-14-016A2), and Development fund for

Graduate Student Education in University of Science and Technology Beijing.

References

1 Z. M. Dang, J. K. Yuan, J. W. Zha, T. Zhou, S. T. Li, and G. H. Hu, *Prog. Mater. Sci.*, 2012, **57**, 660.
2 M. Arbatti, X. B. Shan, and Z. Y. Cheng, *Adv. Mater.*, 2007, **19**,1369.
3 Z. M. Dang, J. K. Yuan, S. H. Yao, and R. J. Liao, *Adv. Mater.*, 2013, **25**, 6334.
4 P. Thomas, K. T. Varughese, K. Dwarakanath, and K. B. R. Varma, *Comps. Sci. Technol.*, 2010, **70**, 539.
5 Z. M. Dang, Y. Q. Lin, H. P. Xu, C. Y. Shi, S. T. Li, and J. B. Bai, *Adv. Funct. Mater.*, 2008, **18**, 1509.
6 L. Y. Xie, X. Y. Huang, Y. H. Huang, K. Yang, and P. K. Jiang, *J. Phys. Chem. C*, 2013, **117**, 22525.
7 B. H. Fan, J. W. Zha, D. R. Wang, J. Zhao, and Z. M. Dang, *Appl. Phys. Lett.*, 2012, **100**, 092903.
8 S. F. Mendes, C. M. Costa, C. Caparros, V. Sencadas, and S. Lanceros-Mendez, *J Mater Sci*, 2012, **47**, 1378.
9 Q. G. Chi, J. Sun, C. H. Zhang, G. Liu, J. Q. Lin, Y. N. Wang, X. Wang, and Q. Q. Lei, *J. Mater. Chem. C*, 2014, **2**, 172.
10 Z. M. Dang, W. Y. Yin, Q. Zhang, and Q. Q. Lei, *Adv. Mater.*, 2007, **19**, 852.
11 Y. K. Yuan, S. H. Yao, and Z. M. Dang, *J. Phys. Chem. C*, 2011, **115**, 5515.
12 B. H. Wang, G. Z. Liang, Y. C. Jiao, A. J. Gu, L. M. Liu, L. Yuan, and W. Zhang, *Carbon*, 2013, **54**, 224.
13 Y. Zhang, Y. Wang, Y. Deng, M. Li, and J. B. Bai, *ACS Appl. Mater. Interfaces*, 2012, **4**, 65.
14 T. Haneman, and D. V. Szabo, *Materials*, 2010, **3**, 3468.
15 Y. Shen, Y. H. Lin, M. Li, and C. W. Nan, *Adv. Mater.*, 2007, **19**, 1418.
16 C. W. Nan, Y. Shen, and J. Ma, *Annu. Rev. Mater. Res.*, 2010, **40**, 131.
17 Y. Kobayashi, V. Salgueiriño-Maceira, and L, Liz-Marzán, *Chem. Mat.*, 2001, **13**, 1630.
18 Electroless Plating: Fundamentals and Applications, ed. G. O. Mallory and J. B. Hajdu, American Electroplaters and Surface Finishers Society, Orlando, 1990, 1st edn., 1990, p. 458.
19 Z. M. Dang, H. Y. Wang, and H. P. Xu, *Appl. Phys. Lett.*, 2006, **89**, 112902.
20 S. D. Vacche, F. Oliveira, Y. Leterrier, V. Michaud, D. Damjanovic, and J. E. Manson, *J Mater Sci*, 2014, **49**, 4552.
21 T. Kojima, M. Sugihara, Y. Hosoi, N. Uekawa, and K. Kakegawa, *J. Ceram. Soc. Japan*, 2009, **12**, 1328.
22 C. Marega, and A. Marigo, *Eur Polym J*, 2003, **39**, 1713.
23 L. Ramajo, M. S. Castro, and M. M. Reboredo, *J Mater Sci*, 2010, **45**, 106.
24 S. H. Yao, Z. M. Dang, M. J. Jiang, and J. B. Bai, *Appl. Phys. Lett.*, 2008, **93**, 182905.
25 D. R. Wang, T. Zhou, J. W. Zha, J. Zhao, C. Y. Shi, and Z. M. Dang, *J. Mater. Chem. A*, 2013, **1**, 6162.
26 X. J. Yang, J. Y. Li, and Y. P. Lei, *Adv. Mater. Res.*, 2013, **668**, 17.
27 R. Berthe, and J. Halbritter, *Phys. Rev. B*, 1991, **43**, 6880.
28 S. Gregory, *Phys. Rev. Lett.*, 1990, **64**, 689.
29 Q. Feng, Z. M. Dang, N. Li, and X. Cao, *Mater. Sci. Eng. B*, 2003, **99**, 325.
30 L. Ren, J. Zhao, S. J. Wang, B. Z. Han, and Z. M. Dang, *Comps. Sci. Technol.*, 2015, **114**, 57.